Available online at www.sciencedirect.com

ScienceDirect

Advances in Space Research 76 (2025) 1225–1239

ADVANCES IN SPACE RESEARCH (a COSPAR publication)

www.elsevier.com/locate/asr

High latitude observation of the Forbush decrease during the May 2024 solar storms with muon and neutron detectors on Svalbard

F. Riggi [l,t,u,1,*], L. Hertle [af,1,*], M. Abbrescia [a,b], C. Avanzini [c,d], L. Baldini [c,d], R. Baldini Ferroli [e], G. Batignani [c,d,l], M. Battaglieri [f], S. Boi [g,h], J. Boike [ag,ah], E. Bossini [d], F. Carnesecchi [i], D. Cavazza [j], C. Cicalò [h], L. Cifarelli [j,k,l], F. Coccetti [l], E. Coccia [m], A. Corvaglia [n], D. De Gruttola [o,p,l], S. De Pasquale [o,p,l], P. Dietrich [af], L. Galante [q], M. Garbini [l,j], E. Gericke [ak], I. Gnesi [l,r], F. Gramegna [w], E. Gramstad [al], S. Grazzi [s,f], E.S. Haland [al], D. Hatzifotiadou [j,i], P. La Rocca [t,u,l], N. Krebs [aj], S. Landmark [af], Z. Liu [v], G. Mandaglio [s,u], A. Margotti [j], G. Maron [w], M. Maturilli [ag], M.N. Mazziotta [b], A. Mulliri [g,h], R. Nania [j,l], F. Noferini [j,l], F. Nozzoli [x], F. Ould-Saada [al], F. Palmonari [k,j], M. Panareo [y,n], M.P. Panetta [n], R. Paoletti [z,d], C. Pellegrino [aa], L. Perasso [f], C. Pinto [i], S. Pisano [l,e], G. Righini [ab], C. Ripoli [o,p,l], M. Rizzi [b], G. Sartorelli [k,j], E. Scapparone [j], P. Schattan [ai,aj], M. Schioppa [ac,r], M. Schrön [af], G. Scioli [k,j], A. Scribano [z,d], M. Selvi [j], M. Taiuti [ad,f], G. Terreni [d], A. Trifirò [s,u], M. Trimarchi [s,u], C. Vistoli [aa], L. Votano [ae], M.C.S. Williams [i,v], S. Zacharias [af], A. Zichichi [i,j,k,l,v], R. Zuyeuski [v,i], O. Pinazza [j,l,i]

[a] *Dipartimento di Fisica "M. Merlin", Universita e Politecnico di Bari, Via Amendola 173, 70125 Bari, Italy*
[b] *INFN, Sezione di Bari, Via Orabona 4, 70126 Bari, Italy*
[c] *Dipartimento di Fisica "E. Fermi", Universita di Pisa, Largo Bruno Pontecorvo 3, 56127 Pisa, Italy*
[d] *INFN, Sezione di Pisa, Largo Bruno Pontecorvo 3, 56127 Pisa, Italy*
[e] *INFN, Laboratori Nazionali di Frascati, Via Enrico Fermi 54, 00044 Frascati (RM), Italy*
[f] *INFN, Sezione di Genova, Via Dodecaneso 33, 16146 Genova, Italy*
[g] *Dipartimento di Fisica, Universita di Cagliari, S.P. Monserrato-Sestu Km 0.700, 09042 Monserrato (CA), Italy*
[h] *INFN, Sezione di Cagliari, S.P. Monserrato-Sestu Km 0.700, 09042 Monserrato (CA), Italy*
[i] *European Organisation for Nuclear Research (CERN), Esplanade des Particules 1, 1211 Geneva 23, Switzerland*
[j] *INFN Sezione di Bologna, Viale Carlo Berti Pichat 6-2, 40127 Bologna, Italy*
[k] *Dipartimento di Fisica e Astronomia "A. Righi", Universita di Bologna, Viale Carlo Berti Pichat 6-2, 40127 Bologna, Italy*
[l] *Museo Storico della Fisica e Centro Studi e Ricerche "E. Fermi", Via Panisperna 89a, 00184 Roma, Italy*
[m] *Gran Sasso Science Institute, Viale Francesco Crispi 7, 67100 L'Aquila, Italy*
[n] *INFN Sezione di Lecce, Via per Arnesano, 73100 Lecce, Italy*
[o] *Dipartimento di Fisica "E. R. Caianiello", Universita di Salerno, Via Giovanni Paolo II 132, 84084 Fisciano (SA), Italy*
[p] *INFN Gruppo Collegato di Salerno, Complesso Universitario di Monte S. Angelo Ed. 6, Via Cintia, 80126 Napoli, Italy*
[q] *Teaching and Language Lab, Politecnico di Torino, Corso Duca degli Abruzzi 24, Torino, Italy*
[r] *INFN Gruppo Collegato di Cosenza, Via Pietro Bucci, Rende (Cosenza), Italy*
[s] *Dipartimento di Scienze Matematiche e Informatiche, Scienze Fisiche e Scienze della Terra, Universita di Messina, Viale Ferdinando Stagno d'Alcontres 31, 98166 Messina, Italy*
[t] *Dipartimento di Fisica e Astronomia "E. Majorana", Universita di Catania, Via S. Sofia 64, 95123 Catania, Italy*
[u] *INFN Sezione di Catania, Via S. Sofia 64, 95123 Catania, Italy*

* Corresponding author.
E-mail addresses: Francesco.Riggi@ct.infn.it (F. Riggi), lasse.hertle@ufz.de (L. Hertle).
[1] F.Riggi and L. Hertle contributed equally to this work.

https://doi.org/10.1016/j.asr.2025.05.023

[v] ICSC World Laboratory, Geneva, Switzerland
[w] INFN Laboratori Nazionali di Legnaro, Viale dell'Universita 2, 35020 Legnaro, Italy
[x] INFN Trento Institute for Fundamental Physics and Applications, Via Sommarive 14, 38123 Trento, Italy
[y] Dipartimento di Matematica e Fisica "E. De Giorgi", Universita del Salento, Via per Arnesano, 73100 Lecce, Italy
[z] Dipartimento di Scienze Fisiche, della Terra e dell'Ambiente, Universita di Siena, Via Roma 56, 53100 Siena, Italy
[aa] INFN-CNAF, Viale Carlo Berti Pichat 6-2, 40127 Bologna, Italy
[ab] CNR, Istituto di Fisica Applicata "Nello Carrara", Via Madonna del Piano 10, 50019 Sesto Fiorentino (FI), Italy
[ac] Dipartimento di Fisica, Universita della Calabria, Via Pietro Bucci, Rende (CS), Italy
[ad] Dipartimento di Fisica, Universita di Genova, Via Dodecaneso 33, 16146 Genova, Italy
[ae] INFN Laboratori Nazionali del Gran Sasso, Via G. Acitelli 22, 67100 Assergi (AQ), Italy
[af] Helmholtz Centre for Environmental Research GmbH - UFZ, Permoserstr. 15, 04318 Leipzig, Germany
[ag] Alfred Wegener Institute Helmholtz Centre for Polar and Marine Research, Potsdam, Germany
[ah] Department of Geography, Humboldt Universitaet zu Berlin, Berlin, Germany
[ai] Institute of Hydrology and Water Management (HyWa), University of Natural Resources and Life Sciences (BOKU), Muthgasse 18, 1190 Vienna, Austria
[aj] Institute of Geography, University of Innsbruck, Innrain 52f, 6020 Innsbruck, Austria
[ak] Bundesamt fur Strahlenschutz, Berlin, Germany
[al] Physics Department, Oslo University, P.O.Box 1048, 0316 Oslo, Norway

Received 14 February 2025; received in revised form 6 May 2025; accepted 8 May 2025
Available online 14 May 2025

Abstract

During the series of intense solar flares and coronal mass ejections, that occurred in May 2024, a remarkable Forbush decrease in the cosmic ray flux was observed on the Earth. While this event was observed by particle detectors around the world, the archipelago of Svalbard was heavily exposed to it due to the weak geomagnetic shielding in the polar region. In this study, an analysis of the Forbush decrease event was carried out with a unique combination of muon and neutron detectors on Svalbard: at Ny-Ålesund three scintillator-based muon telescopes of the Extreme Energy Events (EEE) project, 14 channels of a Bonner Sphere neutron Spectrometer (BSS), and thermal and epithermal neutron sensors used for hydrological monitoring; and, at Barentsburg, a high-energy neutron monitor operated by the Polar Geophysical Institute. Most sensors showed significant responses and correlation during the event. The observed relative magnitude of the Forbush decrease was found to depend on the detector's energy sensitivity and was $\approx 9\%$ for thermal neutrons, $\approx 8\%$ for high-energy neutrons, and $\approx 3\%$ for muons. The uncertainty of these results strongly depends on factors like the count rate, which ranged from 10^1 to 10^5 cph and resulted in a low signal-to-noise ratio particularly for the BSS. These multi-particle and multi-energy observations provide an unprecendented view on the Earth's exposure to cosmic rays during solar events.

Keywords: Forbush decrease; Muon telescopes; Neutron detectors

1. Introduction

A series of intense events consisting of solar flares, coronal mass ejections (CMEs), and geomagnetic storm components has occurred, starting on May 8, 2024, during solar cycle 25. The geomagnetic storm was the largest registered in the last twenty years, after those occurring in October-November 2003 Cid et al. (2015).

These events were observed in conjunction with the formation of an active solar region, named AR13664 by the National Oceanic and Atmospheric Administration, which produced two large and multiple medium solar flares on May 8, together with several Coronal Mass Ejections (CMEs) in the direction of Earth. The size of this region was extraordinary, about 200,000 km in diameter, 15 times larger than the Earth's diameter.

Fig. 1 (center) shows an H-α picture of the AR13664 region on May 10, taken by the Solar Telescope of the INAF Catania Astrophysical Observatory (Romano et al., 2022; INAF, 2024), in Italy, compared to similar pictures taken on May 6 (left) and May 14 (right). The evolution of this region during May 2024, together with several parameters concerning the Sun activity has been recently discussed in Hayakawa et al. (2024) and Kwak et al. (2024).

Solar flares are explosions on the Sun, able to produce a burst of radiation across the electromagnetic spectrum, from radio waves to gamma rays. The usual classification of solar flares is made according to the associated intensity in the wavelength range 0.1 to 0.8 nm, X-flares being the largest, whereas M-flares are medium-sized and C-flares are small-sized. Each category has nine subdivisions, from M1 to M9, or X1 to X9, with a log scale, where the

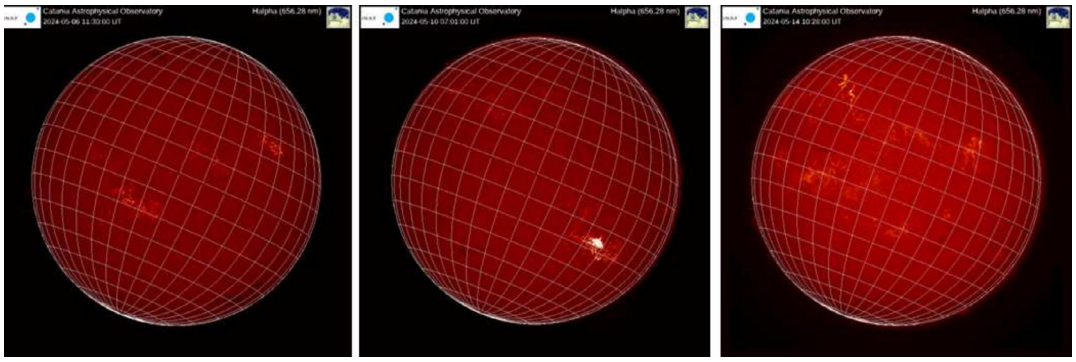

Fig. 1. Picture of the AR13664 region on May 10 (center), as observed by the Solar Telescope of the INAF Catania Astrophysical Observatory (Romano et al., 2022; INAF, 2024), in Italy, compared to pictures taken on May 6 (left) and. May 14 (right).

Table 1
Solar events between May 8–15, 2024 and their main parameters: Magnitude of the observed X-class solar flares and speed of the corresponding coronal mass ejection (CME). The events on May 11th 11:44 and May 12th 16:26 were not accompanied by CMEs. Data taken from Hayakawa et al. (2024).

Peak time (UTC)	Magnitude	CME speed (km/s)
2024–05-08 05:09	X1.0	511
2024–05-08 21:40	X1.0	947
2024–05-09 09:13	X2.2	1226
2024–05-09 17:44	X1.1	1019
2024–05-10 06:54	X3.9	1006
2024–05-11 01:23	X5.8	1512
2024–05-11 11:44	X1.5	–
2024–05-12 16:26	X1.0	–
2024–05-14 02:09	X1.7	929
2024–05-14 12:55	X1.2	792
2024–05-14 16:51	X8.7	1988
2024–05-15 08:37	X3.4	1724

magnitude of X1 is a factor of 10 with respect to M1 and a factor of 100 with respect to C1. X-class flares, together with the corresponding CMEs, are major events which are expected to produce observable effects in different areas of the human activities. They may trigger blackouts on a planetary scale and radiation hazards to people on board of space vehicles.

Additional intense solar flares were then produced in the following days, on May 9 (X2.2 and X1.1-classes), May 10 (X3.9-class), May 11, with two other X-class flares of magnitude 1.5 and 5.8, and on May 12 (X1.0). Finally, additional large flares happened on May 14 (X8.7) and on May 15 (X3.4). A summary of such flares is shown in Table 1. The table reports the magnitude of observed X-class solar flares, together with their peak UTC time and the speed of the associated disturbance propagating towards the Earth. A more complete list is reported in Hayakawa et al. (2024). As it is seen, the evolution of the events is rather complex in comparison to other solar events characterized by a single flare or coronal mass ejection.

The May 2024 storms had a negative impact on ground-based broadcasting and radio communications, especially in the shortwave band. GPS navigation was also affected in a few cases, and some weather satellites stopped transmitting data (Ram et al., 2024). Also the Starlink fleet of low-orbiting satellites experienced some degradation in their performance (Ashrufayisha, 2024).

Forbush decreases in the cosmic ray flux, although not directly associated with solar flares, are one of the observable effects of such events, especially when large solar flares are accompanied by coronal mass ejections. These are among the most important transient variations of the cosmic ray flux observed in the Solar System. Since their discovery (Forbush (1937, 1938)), hundreds of Forbush decreases of various intensity have been observed and catalogued (Lockwood et al., 1990; Cane et al., 1993; Pudovkin and Veretenenko, 1995; Cane et al., 1996), frequently associated with solar flares and interplanetary disturbances. Such variations have been observed not only on the Earth, but also in space, for instance on the MIR and on the International Space Station, in the interplanetary space, on the planet Mars (Freiherr von Forstner et al., 2018; Guo et al., 2018), and up to the border of the Solar System, by the Pioneer 10 & 11 and Voyager 1 & 2 space probes (McDonald et al., 1982). Solar Energetic Particle (SEP) events are bursts of high-energy charged particles – mainly protons, electrons, and heavy ions – originating from the Sun. SEP events vary in intensity and energy spectrum. Smaller events mainly produce electrons and lower-energy protons, while larger events (often associated with fast CMEs) can generate highly energetic protons (>100 MeV) that can penetrate the Earth's magnetosphere, leading to Ground Level Enhancements (GLEs). GLEs are sudden variations which may be observed at the Earth's surface. Contrary to Forbush decreases, they are uncommon events and presently only 76 GLEs have been observed since 1940. One of such events, classified as GLE74, occurred during the period under investigation on May 11 (see Mashao et al., 2024, for instance). Its effects were visible in the neutron monitor data, especially at the Barentsburg site.

Although the topology of Forbush decreases exhibits large differences from event to event, the decrease usually takes place on a time scale of a few hours, and it is observable on the Earth a few days after the solar event (Usoskin et al., 2008). A subsequent recovery to the original value in a time scale of the order of a few days, with a nearly exponential shape, is generally observed in the simplest cases. Forbush events with magnitude larger than 3% are usually regarded as strong events.

The observation of Forbush decreases is generally carried out by means of Neutron Monitor (NM) stations which are distributed throughout the world, and have been measuring the neutron flux for over 70 years. Most of them make their data easily accessible on the web (NMDB, 2024).

As an example, Fig. 2 shows the May 2024 Forbush event as observed by multiple NM stations located in Thailand (2565 m a.s.l.), Mexico (2274 m a.s.l.) and Barentsburg, Spitsbergen (80 m a.s.l), at different altitudes and geomagnetic cutoff rigidities. A relative scale was used to plot the trend from May 1 to 31, with respect to the average evaluated in the quiet pre-Forbush period (May 1–10). Shown in the plot is also the result observed with the Neutron Monitor located at Barentsburg, not far from Ny-Å lesund, in the Svalbard archipelago, where part of our observations were made, characterized by a low geomagnetic cutoff rigidity. It is generally known that Forbush decreases may exhibit a large variety of time profiles, depending on the solar and interplanetary situation (Belov, 2008). Although the sudden decrease is rather similar for all stations, the recovery phase exhibits different details from station to station, as a consequence of the energetic dependence of the Forbush decrease and of the local (magnetospheric and atmospheric) environment of the individual detectors. Moreover, in all stations, large differences with respect to a simple monotonic exponential trend were observed in this case, also due to multiple solar events and CMEs in the period under examination, as reported in Table 1. Due to the common origin of the flux variations at the different stations, such variations are expected to dominate over the statistical fluctuations, especially during the Forbush decrease period. As a check, we evaluated the Pearson correlation coefficient for the three pairs of stations PSNM–MXCO, PSNM–Barentsburg and MXCO–Barentsburg (shown in Fig. 2). We considered the data in 1-h steps, discriminating between the pre-Forbush period (before May 10) and during the first phase of the Forbush event (May 10–15). A high correlation ($r = 0.75 - 0.90$) between any pair was found during the Forbush event, whereas r was compatible with zero in the pre-Forbush period. This also suggested a method for investigating neutron-neutron and muon-neutron correlations across the various time series of the measured rates, that will be discussed in Section 3.

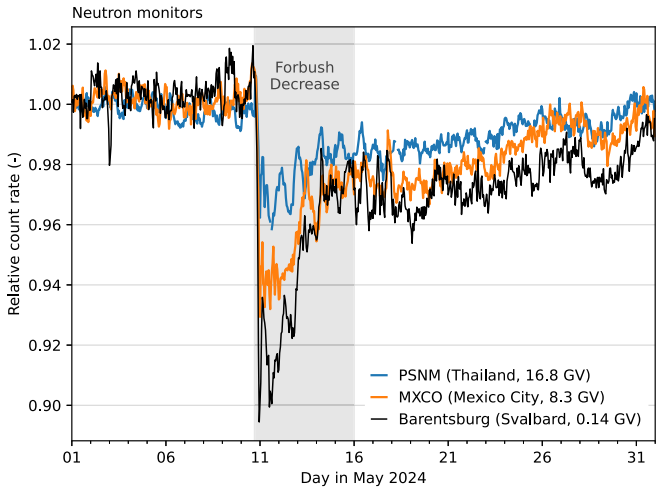

Fig. 2. The May 2024 Forbush decrease event, as observed by multiple neutron monitor stations located in Mexico, Thailand, and Barentsburg, at different altitude and geomagnetic cutoff. A relative scale is used, showing variations with respect to the average evaluated over the quiet pre-Forbush period. Data were retrieved by the Neutron Monitor Data Base (NMDB, 2024) and the Barentsburg site (IZMIRAN, 2024).

The magnitude of the Forbush decrease is the largest for the neutron monitors located at low geomagnetic cutoff. Such magnitude generally depends on several factors, and it is especially sensitive to the energy of the primary cosmic rays producing the particles observed in the detectors. In the case of muons, the dependence of the magnitude reduction on the primary energy may be obtained from the muon flux angular distribution. As an example, data obtained from the URAGAN muon hodoscope (Barbashina et al., 2011) show an amplitude dependence on the median primary energy which may be fitted by a power law $E^{-\alpha}$ above 10 GeV, with α of the order of 1. The shielding provided by the Earth's magnetic field is characterized by the geomagnetic cutoff rigidity, stating if a primary particle may penetrate the magnetosphere, reaching the top of the atmosphere in a given location. This is maximal in the equatorial regions, up to about 17 GV, and almost negligible close to the magnetic poles. There is also an effective atmospheric cutoff for cosmic rays detected at ground, which can be defined as the minimum energy of a cosmic ray primary particle needed to produce secondaries reaching the ground with non-negligible probability and is of the order of 1 GV. While the geomagnetic cutoff is higher than the atmospheric cutoff over most of the Earth surface, the latter may become dominant in the polar regions. The atmospheric cutoff decreases with the altitude, thus providing a better sensitivity to low energy particles for high-altitude detection stations located at polar latitudes (Poluianov and Batalla, 2022). The geomagnetic cut off rigidity plays an important role in determining the magnitude of the observed Forbush decrease (Lockwood, 1971). It must be also remembered that the cosmic ray cutoff terminology has significantly evolved since the early understanding of the magnetospheric transport and that more detailed approaches and definitions of the relevant terms have been discussed (Cooke et al., 1991).

Recent studies have investigated the dependence of Forbush decrease on the geomagnetic cutoff rigidity and

analysed a number of Forbush events observed by multiple NM stations (Okike and Nwuzor, 2020; Nwuzor et al., 2024). They confirm that the Forbush decrease amplitude depends on the station cutoff rigidity. Such studies demonstrate, however, that a number of other factors, such as atmospheric depth, latitude effects and other causes may also influence the cosmic ray intensity variation in a given location (Nwuzor et al., 2024).

For muon telescopes, the observed effect is generally smaller than for neutrons, and a decrease of approximately one-half of that for a neutron monitor at the same cutoff rigidity is expected (Lockwood, 1971). Moreover, detecting muons of higher energy selects on average higher-energy primaries, so the expected effect becomes smaller.

The EEE (Extreme Energy Events) Project is a widespread network of cosmic-ray telescopes with both educational and scientific goals (Abbrescia et al., 2018) since its early phase in 2004. Most of the detectors of the EEE network are made of Multigap Resistive Plate Chambers (MRPC), which have good tracking capabilities, installed in high school environments across Italy and in a few Research and University Institutions, including CERN. Since 2018, additional, scintillator-based telescopes (POLA-R detectors) have been also installed at Ny-Å lesund.

Forbush events have been previously observed by several MRPC telescopes of the EEE network (Abbrescia et al., 2011; Abbrescia et al., 2015). The first observation of a Forbush decrease obtained by the EEE network followed the large X2 solar flare of mid-February 2011 (Abbrescia et al., 2011). From time to time, additional Forbush events were observed and measured by the EEE network of MRPC telescopes, demonstrating their capability to monitor the decrease of the muon cosmic ray flux in such circumstances.

The Svalbard archipelago also hosts several neutron detectors, which include the Neutron Monitor located at Barentsburg (IZMIRAN, 2024; NMDB, 2024), a Bonner Sphere Spectrometer in Ny-Ålesund (Rühm et al., 2009; Pioch et al., 2011; Bittner, 2022), and additional low-energy neutron sensors for monitoring soil and snow water changes (Zreda et al., 2012; Schrön et al., 2018; Schattan et al., 2019).

Due to the relevance of the solar events occurring in May 2024, and the availability of data both from muon and neutron detectors installed at the same high-latitude site, a combined analysis of the information originating from such detectors was made and discussed in the present paper.

Additional analyses which will include the data collected by the network of MRPC muon detectors deployed throughout Italy at different latitudes, as well as data from other neutron detectors, will be discussed in a future work.

Section 2 describes the experimental detection setup and the working conditions, while Section 3 reports the data and the analysis carried out.

2. The muon and neutron detectors used in the present investigation

2.1. The Ny-Ålesund observation site

The Svalbard archipelago is located in the Arctic, between the Greenland Sea and Barents Sea, halfway between the northern coast of Norway and the North Pole. The islands of the archipelago lie from 74° to 81° N, and more than 50% of their surface is covered with glaciers. The largest island is Spitsbergen, on the northwest coast of which is the permanent research site of Ny-Ålesund at 78° 55' 30" N 11° 55' 20" E. While the Norwegian Polar Institute has the role of being Norway's host at the research site, the infrastructure is owned and operated by Kings Bay, a Norwegian government enterprise, which provides permanent research facilities to many scientific institutions from different countries. Among these, the Dirigibile-Italia Station (CNR), the Amundsen-Nobile Climate Change Tower and the Gruvebadet Laboratory are the buildings where the three POLA-R telescopes have been installed for a long-term measurement campaign.

The location of the three stations where the muon detectors are installed is shown in Fig. 3. The relative distances between the three detectors are shown in the picture and are about 730 m, 930 m and 1270 m. These distances allow for the observation of coincidence events, although with a low rate, due to the detection of extensive air showers.

The Bonner Sphere Spectrometer (BSS) is located in the Blue House of the AWIPEV Research Base, operated jointly by the German Alfred Wegener Institute (AWI) and the French Polar Institute (IPEV), very close to POLA-03. The Cosmic Ray Neutron Sensors (CRNS) detect epithermal and thermal neutrons and are located approximately 700 m west from POLA-01.

Details on the various detectors used are given in the following.

2.2. The POLA-R detectors

In 2018, the almost 60 MRPC telescopes of the EEE Project were complemented by a set of small scintillator-based telescopes which have been then used in various measurement campaigns across Europe, seaborne measurement campaigns in the Arctic and the Mediterranean, and (three of them) installed for several years at Ny-Ålesund. Since the POLA-R scintillator telescopes were already described in previous papers (see for instance Abbrescia et al., 2020), only a brief description will be given.

Each POLA-R detector is made of two planes of plastic scintillators, each with 4 tiles of (30×20) cm^2, separated by a vertical distance of 11 cm. The overall sensitive area of each detection plane is (40×60) cm^2, the external volume is about $(78 \times 56 \times 30)$ cm^3 and its total weight is about 50 kg. The scintillation light produced in each tile by the passage of ionizing particles is read out by a pair of silicon

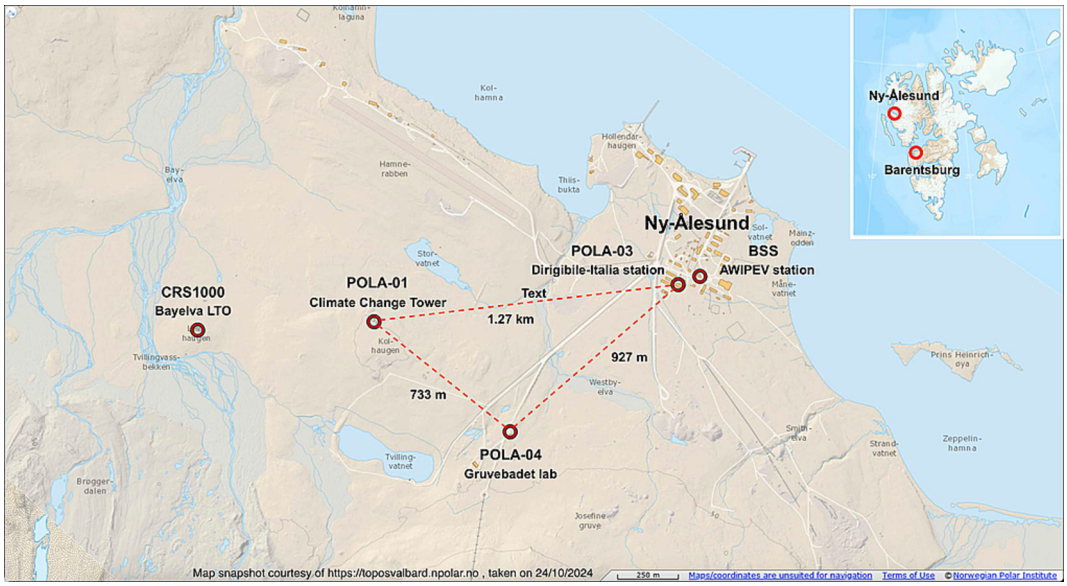

Fig. 3. Map of the Ny-Ålesund site on Svalbard, courtesy of the Norwegian Polar Institute (Norwegian Polar Institute, 2024). Marked in the figure are the locations of the muon and neutron detectors used for the observation of the May 2024 Forbush decrease. The inset also shows the location of Ny-Ålesund and Barentsburg in the Svalb.ard archipelago.

photomultipliers (SiPM). Fast electronics and slow control for the detection operation are embedded in a box below the detector. The trigger for the data acquisition is provided by a coincidence between the top and bottom planes, with at least three signals from different SiPMs. Various environmental sensors (of temperature, pressure, etc.) and a GPS-based synchronization system complement each detector.

The detection efficiency of these detectors had been measured against an external detector able to track particles from the secondary cosmic radiation, mostly GeV muons and energetic (>10 MeV) electrons, and it was found to be around 97%. A more detailed description is reported in Abbrescia et al. (2020).

Apart from short breaks or malfunctioning, which required on-site interventions, the three detectors installed at Ny-Ålesund have been running since 2019, accumulating now about six years of collected data, resulting in more than 10 billion recorded events. Several data analyses are in progress, especially to investigate the annual and solar modulation in the cosmic ray flux, and the coincidence events among the three detectors, originated in extensive air showers.

For the present analysis, data from the POLA-R detectors were corrected by the effect of the atmospheric pressure, which was monitored in short time steps by each station by pressure sensors.

Fig. 4a shows one of the POLA-R detectors installed at Ny-Ålesund.

2.3. The Bonner sphere neutron spectrometer

The Bonner Sphere Spectrometer (BSS) installed at Ny-Ålesund and used for this analysis is made up of 14 spherical neutron detectors, shown in Fig. 4b. Detectors of this type are typically used to reveal temporal variations across the full range of the neutron energy spectrum (Leuthold et al., 2007; Hubert, 2024). Each sphere contains

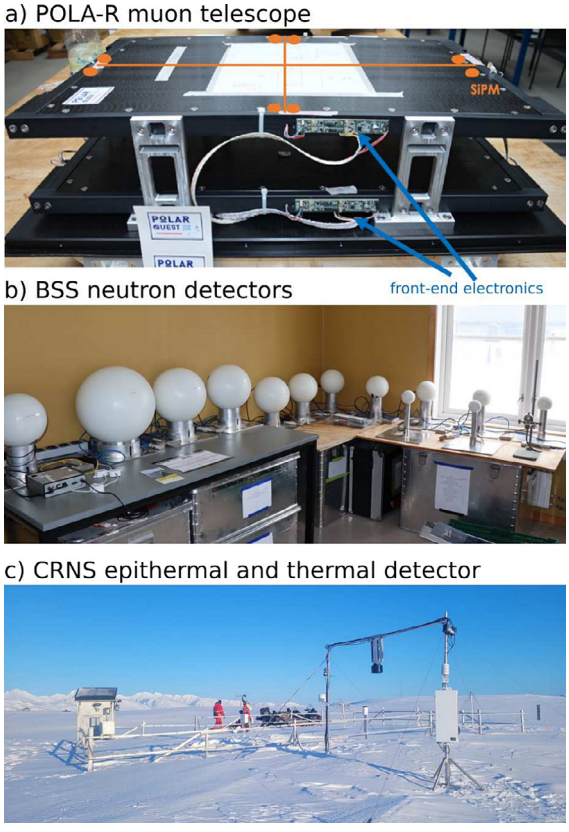

Fig. 4. a) One of the POLA-R muon detectors installed at Ny-Ålesund. The orange dots mark the position of the SiPM devices on opposite corners of the four scintillator plates. b) The Bonner Sphere Spectrometer (BSS) installed at Ny-Ålesund, c) The cosmic-ray neutron sensors (CRNS) installed at the Bayelva site at the outskirt of Ny-Ålesund.

a helium-3 thermal neutron detector. Most He-3 detectors are embedded in a hollow sphere of high-density polyethylene (HDPE) functioning as moderator. The thickness of the HDPE layer varies gradually, influencing the neutron-energy dependent sensitivity of the detectors. Each sphere is referred to by their respective diameter in inches, one detector is bare and one of the 9" detectors bears an additional lead liner resulting in a sensitivity to high energy (> 10 MeV) neutrons. The BSS was installed at Ny-Ålesund in 2007 (Rühm et al., 2009) and has been active in the current configuration since April 2024.

Ancillary sensors also monitor atmospheric pressure, humidity and temperature. The data has been corrected for changes in atmospheric pressure.

2.4. The thermal and epithermal neutron sensors

A Cosmic Ray Neutron Sensor (CRNS) of type CRS1000 (Schrön et al., 2018) was installed at the Bayelva permafrost long term observatory (LTO) in July 2023 to monitor soil moisture and snow water equivalent in the context of the Svalbard Environmental Neutrons project (SVEN). The CRNS consists of two helium-3 neutron detectors, one shielded with 2.5 cm of high density polyethylene and the other without shielding (bare). The shielded detector tube mainly measures neutrons in the epithermal region, while the bare detector mainly measures neutrons in the thermalised peak. Additionally, other sensors also measure atmospheric pressure, humidity and temperature. Usually, the data would be corrected for atmospheric pressure and humidity, but to keep the data processing consistent with the POLA-R and BSS, only pressure was corrected.

Furthermore, the Bayelva LTO sensors monitor various environmental parameters (Boike et al., 2018), such as point-scale soil moisture at different depths, snow height on point-scale, and snow water equivalent. The installed detectors and the Bayelva LTO are shown in Fig. 4c.

Table 2 lists the detector systems used in this study, sorted by their dominant sensitivity to cosmic-ray secondary particle energy. Although there is a large overlap of detector energy sensitivities, the sensitivity of the Bonner Sphere Spectrometer is mainly defined by their sphere sizes (i.e., thickness of plastic shielding). While the bare detector is mainly sensitive to thermal neutrons, small spheres (2–5 cm diameter) detect epithermal to low-energy fast neutrons (0.1 eV to 100 keV), medium spheres (5–15 cm diameter) are sensitive to fast neutrons in the 100 keV to a few MeV range, and large spheres (15–30 cm diameter) extend the sensitivity to high-energy neutrons, typically 1 MeV to 20 MeV. Large spheres with lead lining enhance detection of high energy neutrons, up to hundreds of MeV (Mares and Schraube, 1994; Pioch et al., 2011). Neutron monitors are most sensitive to secondary neutrons in the energy range of 1 MeV to a few GeV, with larger sensitivity in the 100 MeV to 1 GeV range (Clem and Dorman, 2000).

Table 2
Detector systems used in this study, sorted by their sensitivity to energy of cosmic-ray secondary particles, their spherical diameter (only applicable for BSS), and the thickness of the neutron detector's polyethylene shields (HDPE) and the inner lead shields, both in mm. The Barentsburg NM system is also included in the table. The shielding provided are approximate numbers for a standard NM64 (proportional counter filled with BF_3 gas.)

Detector	Diameter	HDPE (mm)	Lead (mm)
CRNS1 (bare)	–	–	–
BSS 1 (bare)	2″	–	–
BSS 2	2.5″	6.4	–
BSS 3	3″	12.7	–
CRNS2 (epith.)	–	25.4	–
BSS 4	4″	25.4	–
BSS 5	5″	38.1	–
BSS 6	6″	50.8	–
BSS 7	7″	63.5	–
BSS 8	8″	76.2	–
BSS 9	9″	88.9	–
BSS 10	10″	101.6	–
BSS 11	11″	114.3	–
BSS 12	12″	127.0	–
BSS 13	15″	165.1	–
BSS 14	9″	63.5	25.4
NM	–	103.0	137.0
POLA-01	–	–	–
POLA-03	–	–	–
POLA-04	–	–	–

Finally, the POLA-R scintillator telescopes measure cosmic ray charged particles, which are mostly muons, with an average energy of 4 GeV at ground level, and some fraction of energetic electrons, with typical energies > 10 MeV (Grieder, 2023).

3. Experimental results

For the present investigation we considered the data collected in May 2024 by the three POLA-R detectors, by the Bonner Sphere Spectrometer (BSS) and by the epithermal and thermal neutron sensors (CRNS), as described in the previous Section.

3.1. Environmental influences

Lower energy neutron detectors, such as the epithermal and thermal neutrons, are highly sensitive to hydrogen abundance in the surrounding environment, such as soil water content and snow (Köhli et al., 2015). Cosmic muon flux has also been shown to have some correlation with temperature (Verpoest et al., 2024). Seasonal variations of atmospheric muons have been traditionally interpreted as due to a variation in the effective temperature, which summarize the atmospheric temperature profile, hence modifying the density in the upper atmosphere and the muon production probability. This effect could be however particularly relevant only for high energy muons (energies higher than the critical energy for pions, 115 GeV, and for kaons, 857 GeV), while the correlation with temperature is expected to be small at low energies. Therefore, it

is imperative to monitor possible changes in environmental parameters during the observed Forbush and quiet periods. The relevant parameters here are atmospheric temperature, atmospheric humidity, atmospheric pressure, and snow water equivalent (near the neutron detectors). Atmospheric temperature and humidity can be obtained from the daily balloon-borne atmospheric soundings carried out at Ny-Ålesund (Maturilli, 2024). The temperature is averaged over the entire atmospheric profile and from the specific humidity the total atmospheric water column can be calculated. As already mentioned in Section 2, atmospheric pressure is monitored at each detector. Snow depth data is measured in the Bayelva LTO. It can be seen in Fig. 5 that the relevant environmental parameters, excluding atmospheric pressure for which variations were taken into account, do not exhibit trends that align with the timescale of the Forbush event as shown in the muon and neutron data. Therefore, the observed decrease is unlikely to be caused by environmental effects. Due to the coarse resolution of the atmospheric data, environmental influences on sub-daily timescales can not be wholly excluded. Thus, changes in the measured neutrons and muon rates can be attributed to the solar events.

3.2. Cosmic ray rates and Forbush decrease magnitude

The pressure-corrected trends of the cosmic ray rate measured by the three POLA-R detectors (top), the BSS detectors (middle) and the CRNS detectors (bottom) are shown in Fig. 6 for the period May 1–31. The POLA-R

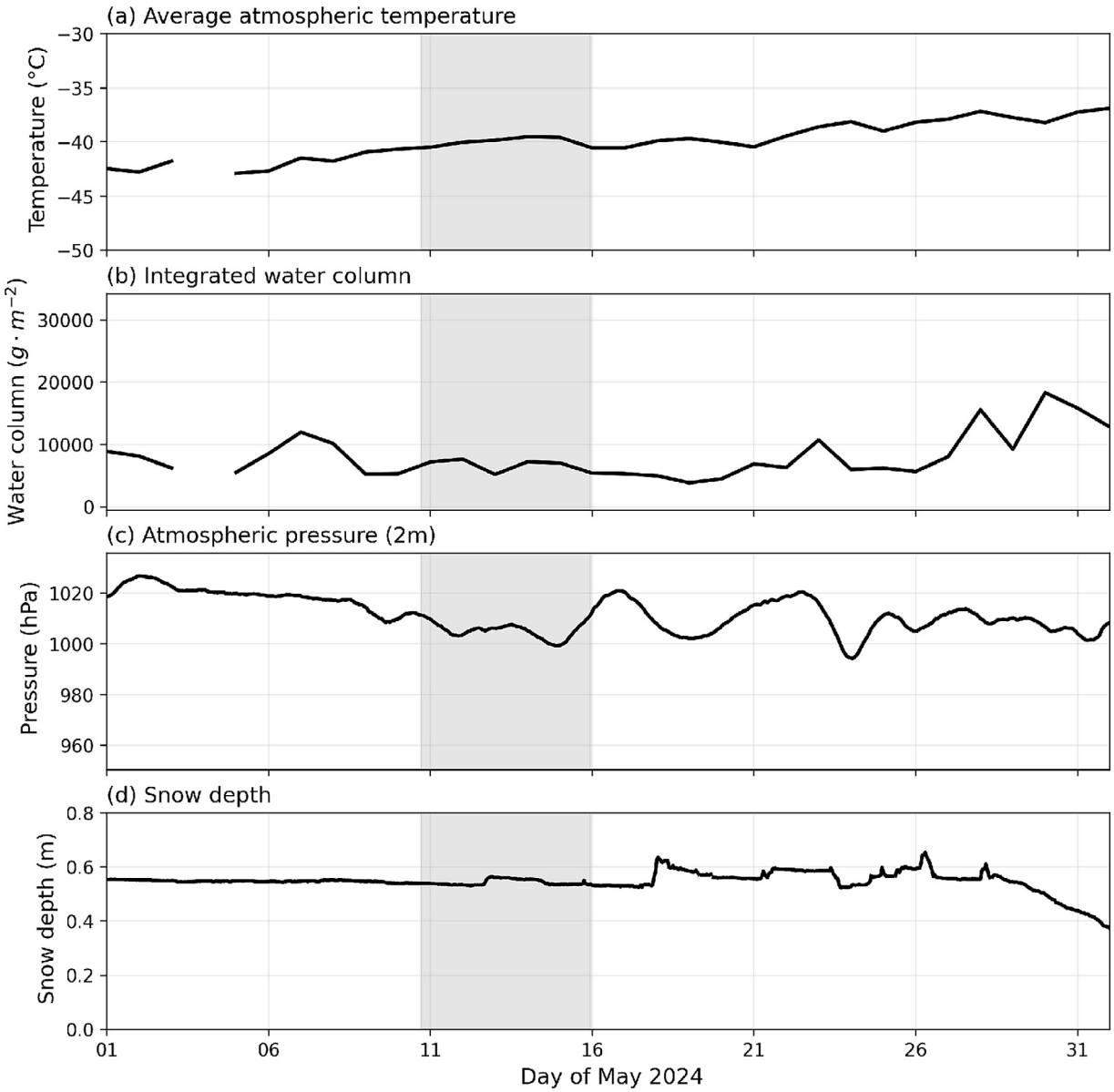

Fig. 5. Potentially influencing environmental variables measured at the Bayelva long-term observatory in May 2024: (a) atmospheric temperature, (b) integrated water column, both taken from (Maturilli, 2024), (c) atmospheric pressure at 2 m height observed by the CRNS and (d) snow depth. The time period corresponding to the Forbush event is. shaded in grey.

and CRNS data were integrated in time steps of 1 h and the BSS data were integrated over 6 h intervals, due to the lower count rates.

The three groups of detectors operate at distinct magnitudes of count rates, the POLA-R detectors operate at approximately $1 \cdot 10^5$ Cts h^{-1}, the BSS between approxi-

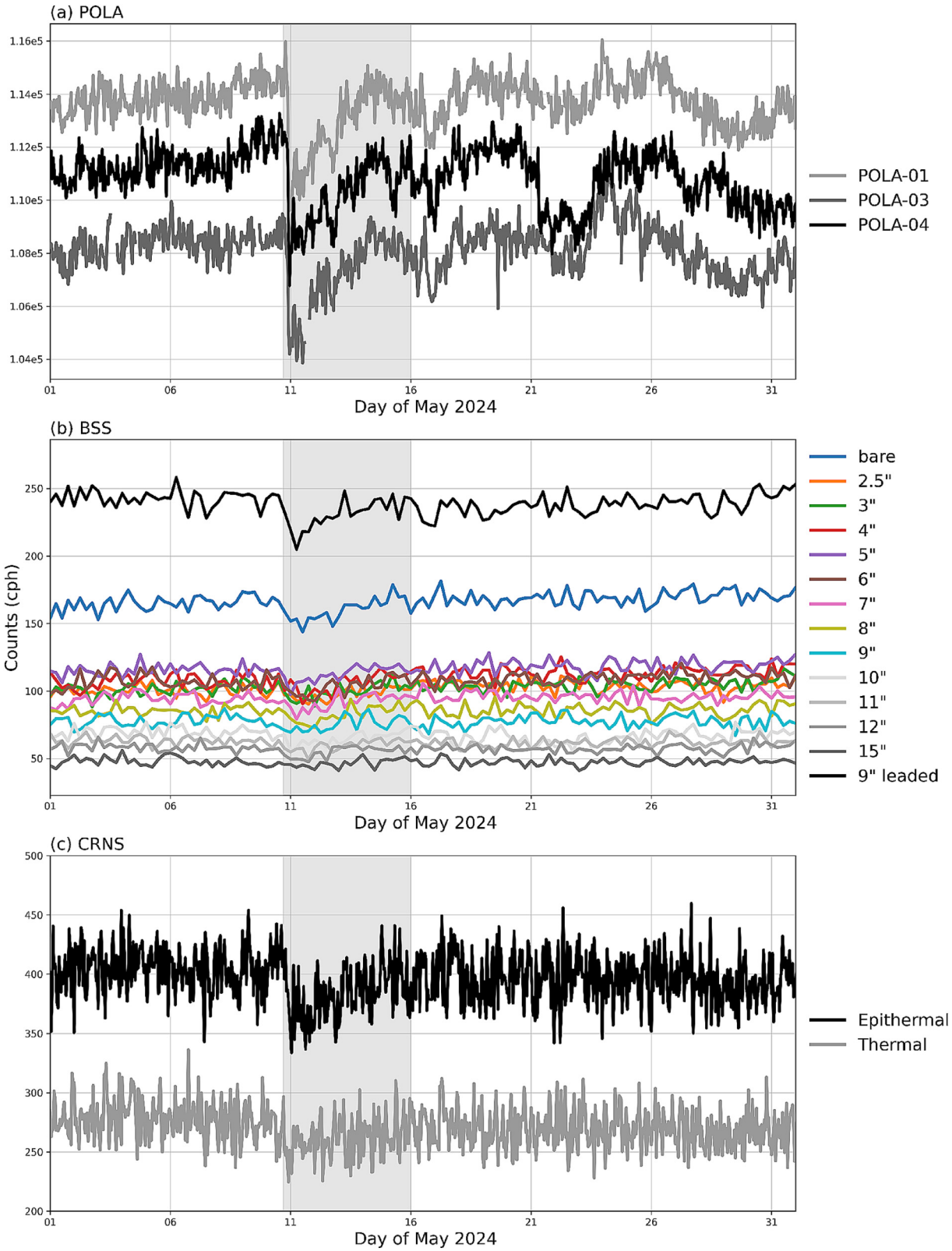

Fig. 6. Pressure-corrected (a) muon rates measured by the POLA-R detectors, (b) neutron rates observed by the BSS and (c) by the CRNS detector. The BSS data is shown in 6 h time steps, while the CRNS and POLA-R data are shown in 1 h intervals. The Forbush period is shaded in grey.

mately 50 and 250 Cts h^{-1} and the CRNS at approximately 400 and 275 Cts h^{-1}.

The differential rate of each individual detector, including the Barentsburg neutron monitor, is shown in Fig. 7, which shows the relative variation with respect to the average evaluated between May 1–31 integrated to 6 h time steps.

The three POLA-R detectors exhibit a high degree of similarity throughout the entire month, the only exception is a decrease in POLA-04 between the 21st and 25th of May, which is not observed by the other two detectors to the same extent.

An abrupt decrease is observed, in most detectors on May 10th at around 17:00 UTC, the time of onset being

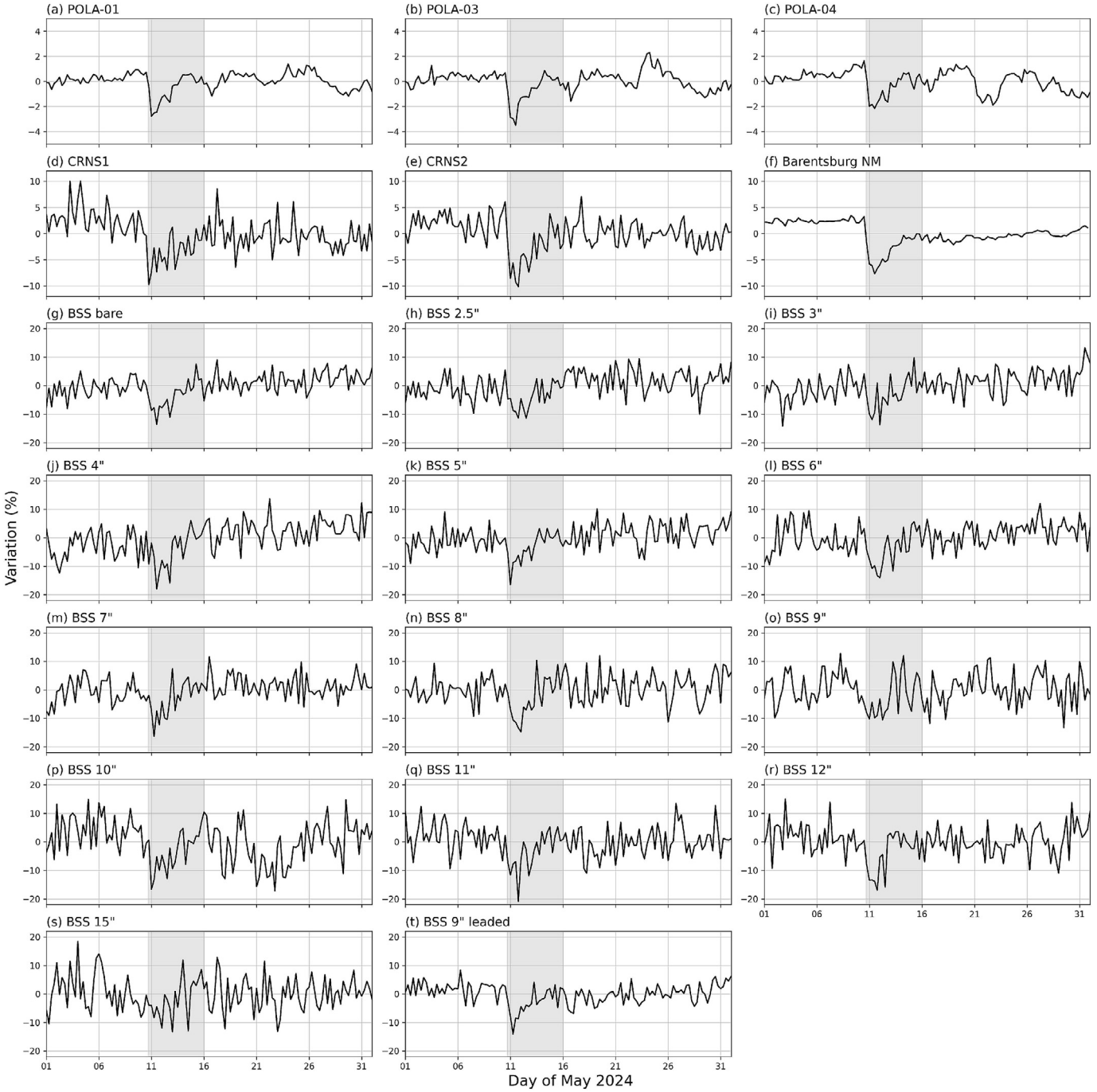

Fig. 7. Differential count rates (percent variations with respect to the average) aggregated over 6 h for the various detector systems: (a-c) POLA-R detectors, (d,e) CRNS thermal and epithermal detectors, (f) Neutron Monitor (NM) at Barentsburg, (g-t) BSS spheres. The Forbush decrease period is shaded in grey.

consistent between all detectors. The exceptions are the 9” and 15” BSS, where the 9” sphere seems to show an earlier onset and the 15” sphere does not show an obvious disturbance.

Forbush decrease magnitudes for all detectors were calculated using the a method similar to Light et al. (2020) and are shown in Fig. 8 with their stochastic measurement errors. The magnitude was defined to be

$$\text{Magnitude} = \frac{\text{Max} - \text{Min}}{\text{Max}}. \quad (1)$$

In Eq. (1) Max and Min are the average of 24 h of data immediately before and after the onset of the Forbush decrease.

The magnitude observed in the neutron measurements is considerably larger than the one observed for muons. The POLA-R detectors observe a magnitude of approximately 2.7 %, the neutron monitor 8 % and the CRNS channels at approximately 9 %. The POLA-R detectors are in good agreement among each other, the maximum variation between them is 0.3 %. Table 2 shows that both bare neutron detectors (CRNS1 and BSS bare) have the same shielding and thus should show similar reactions, which is indeed reflected by agreement in the magnitude. The same is true for the two epithermal neutron detectors, CRNS2 and BSS 4”. The leaded 9” sphere responds to a similar energy spectrum like the neutron monitor in Barentsburg, which is also confirmed by the observed magnitude. It has to be noted that the magnitudes calculated for the BSS carry a large error due to the low count rates and high fluctuations of the system itself as shown in Fig. 7. As previously observed, the 15” sphere shows little response and the error even extends into a magnitude below 0, which would indicate an increase during the Forbush decrease. Still, there is a noteable trend among the BSS towards higher magnitudes as the shielding increases, observable between the 6” and the 12”.

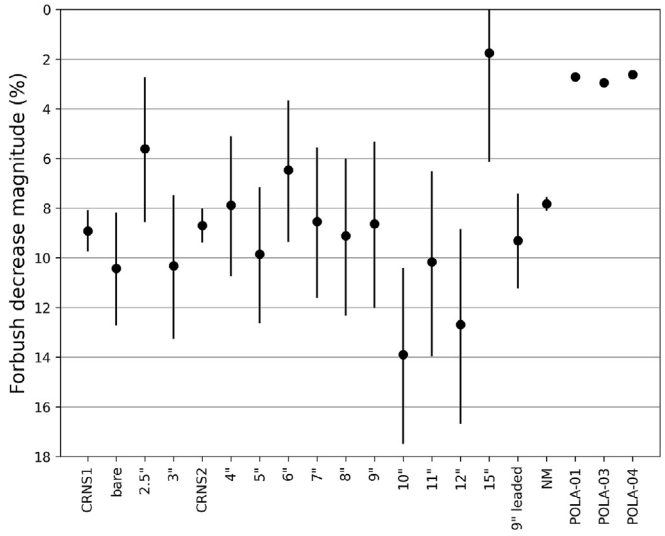

Fig. 8. The magnitude (dip size) of the Forbush decrease event as observed by the individual detectors with associated stochastic measurement errors. Errors on muon data are within the size of the symbols. Similar to Table 2, the detectors are arranged in ascending order of co. smic ray energy.

In order to evaluate the recovery phase of all detectors the time series were separated into three distinct periods, referred to as the quiet phase, the Forbush phase, and the recovery phases. The Forbush period is shaded grey in Figs. 6 and 7. The quiet and recovery phase are the period in May preceding and following the Forbush phase, 01.05.2024–10.05.2024 and 16.05.2024–31.05.2024 respectively, now the magnitude of the recovery phase is calculated with regards to the quiet phase using Eq. (1). Again there are trends discernible, POLA-01, POLA-03 and POLA-04 return within the defined recovery phase to their pre-Forbush rate. The Barentsburg neutron monitor and the CRNS detectors both do not return to their pre-Forbush rate within the recovery phase, this indicates that their recovery times are longer than that of the POLA-R detectors. As already shown in Section 1, the AR13664 region had a complex evolution for the period after the main event, even after the 14-days half-rotation period of the Sun, when the region faced the Earth again (Hayakawa et al., 2024). This was accompanied by additional CMEs around mid May (see Table 1). A long recovery phase for neutron measurements is observed, although it is not straightforward to put it in close connection with the sequence of additional disturbances in the following days. It is interesting to note that additional strong flares from X5 to X12 (on May 20) accompanied by massive CMEs were observed by the Solar Orbiter during the period when the active region was hidden from the Earth view, watching the Sun from the opposite side at that time. The CME on May 20 was so huge that its effect was even observed from the Earth side by the ESA/NASA SOHO mission. Moreover, another CME was observed by the SOHO mission on May 27, and, although not directed towards the Earth, it resulted in strong radio blackouts observed in North America. It is further notable that this extended recovery phase is not observed with the same features in the muon measurements. The same is also true for the BSS with diameters below 9”, these low energy spheres even exceeded the pre-Forbush count rate within the recovery period, which is likely due to statistical fluctuations. The more shielded spheres follow the trend observed in the magnitude, with comparable evolution to the neutron monitor.

Considering the general similarity of the three POLA-R detectors, and the close proximity to each other, we used the overall muon count rates to investigate for their correlations with the neutron detectors.

3.3. Correlation analysis

A correlation analysis was first conducted among the three possible pairs of POLA-R detectors. Similarly to what has been observed for different neutron monitor stations (see Fig. 2), a high degree of correlation was found during the Forbush period for the POLA-01-POLA-03

pair, with a Pearson coefficient of $r = 0.85$. This is in contrast to the quiet period with a Pearson coefficient of $r = 0.27$, both shown in Fig. 9. Similar results were also found for the other possible pairs of POLA-R detectors.

To investigate the muon-neutron correlation, we considered the two time series originating from the average rate of the three POLA-R detectors and from the neutron rate of the Barentsburg NM detector. While the correlation between them is negligible in the pre-Forbush period ($r = 0.25$), a high degree of correlation ($r = 0.88$) is observed during the Forbush period (Fig. 9, top right), pointing out that the muon rate and the rate of neutrons detected by the Barentsburg NM detector, which is sensitive especially to primary cosmic rays in the 0.5–20 GeV range, are highly correlated.

The same approach was adopted to investigate the correlation between muon data and neutron data from the various channels of the BSS at Ny-Ålesund, as well as from the CRNS sensors, discriminating between the results obtained in a quiet period preceding the Forbush event (before May 10) and during the Forbush event (May 10–15). As an example, Fig. 9 (bottom left and right) shows the correlation plots between muons, averaged over all three POLA-R detectors, and the two individual BSS1 and BSS14 channels, corresponding to the lowest and highest BSS neutron energies, aggregated in 6-h steps, during the pre-Forbush and the Forbush periods. It cannot be excluded that some residual variations could be explained by local effects in the vicinity of the Bonner Spheres, such as activities in the building, the asymmetric geometry of the sphere arrangement in the room, possible interference between detectors, and the environment inside and outside the building.

To have a complete overview of the correlation features between data taken by the muon detectors and the various neutron detectors, we show in Fig. 10 the complete set of r-values. Again, the correlation coefficients of the muon-neutron are much larger during the Forbush event with

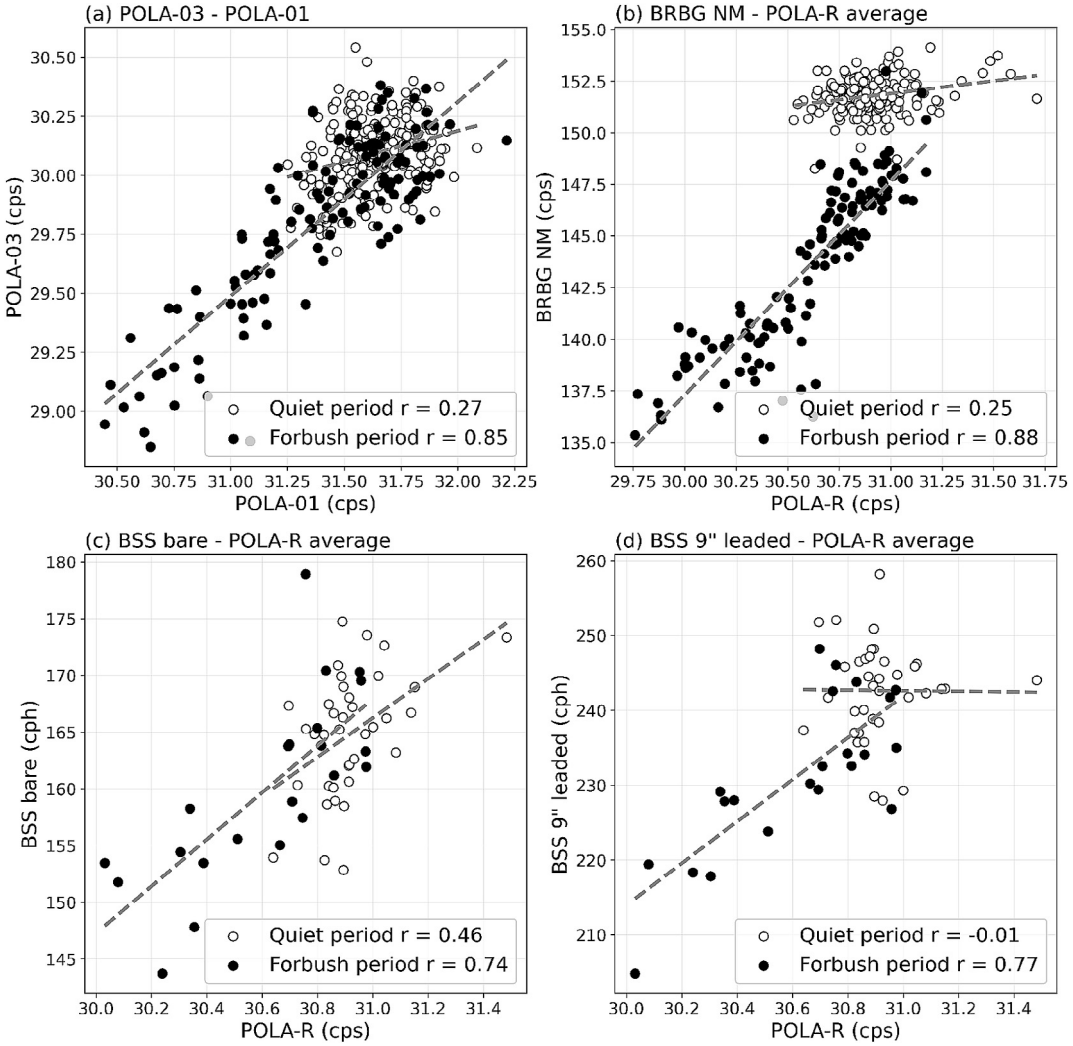

Fig. 9. Count per second (cps) rate correlations between various detectors: (a) POLA-01 and POLA-03; (b) average POLA-R and Barentsburg NM; (c) average POLA-R and BSS bare; (d) average POLA-R and BSS 9" leaded. In (a) and (b), data are aggregated to 1 h intervals, in (c) and (d) to 6 h intervals. Dashed lines are linear fits with the given correlation.

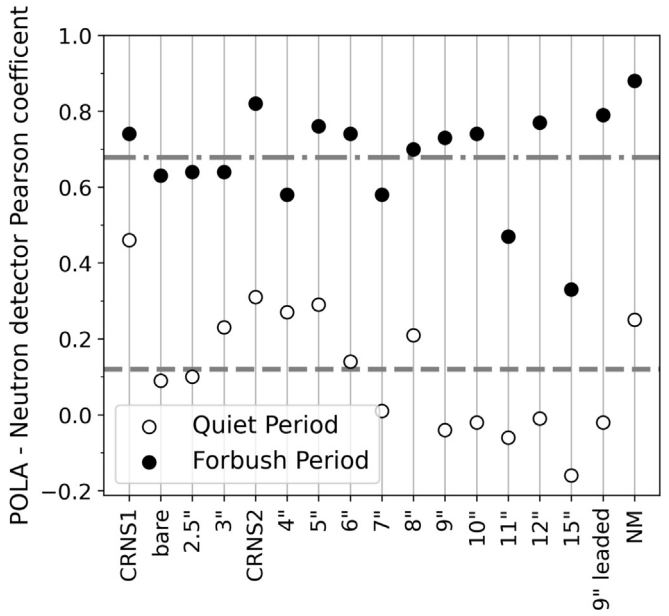

Fig. 10. Correlation coefficients, with respect to the average POLA-R rate of muons, of the neutron rates in the different BSS detector channels, as well as in the CRNS detectors, in the pre-Forbush and Forbush periods. The data, all collected at Ny-Ålesund, are aggregated into 6 h intervals. The dashed lines superimposed show the mean values of the correlation coefficients obtained in the two periods.

respect to the quiet period. It is important to note that most BSS detectors, no matter their size and shielding, show a clear correlation with the POLA-R detectors. Thus, it is not possible to make a reliable statement about the spectral dependence of such a correlation. A clear trend is obvious, the higher the count rate of a specific neutron detector, the higher its correlation with the muon detectors will be. The assumed limit of this dependence would be correlation of the neutron monitor and the POLA-R detectors as statistical fluctuations become negligible in both detectors due to their high count rates.

The pattern of negligible correlation during the quiet period and high correlation during the Forbush event is to be expected. In the absence of short term space weather events the short term time series is dominated by environmental influences and statistical fluctuations. High correlations during quiet periods should be obtainable if timescales of the magnitude of the solar cycle are compared.

4. Conclusions

The Forbush decrease which followed a series of solar flares and coronal mass ejections in May 2024 was observed for the first time by three independent muon detectors installed at the high latitude site of Ny-Ålesund and by different neutron detectors, sensitive to neutrons of various energies, located in the same site or nearby in Barentsburg on the same island of Spitsbergen.

All these detectors have observed the Forbush decrease following the solar events in May 2024. Variations on the cosmic ray flux measured by the various detectors have been observed with different magnitudes and different recovery phases.

A correlation analysis was carried out among the various time series of the measured muon and neutron fluxes to disentangle the effects of the standard long-term correlation between independent cosmic ray detectors in a quiet period (i.e. that arising from cosmic ray variations over a long time scale) from the higher correlation observed during a Forbush event. A strong correlation between the data measured in Ny-Ålesund by the muon telescopes and those provided by the Barentsburg NM station, as well as by the various channels of the Ny-Ålesund Bonner Sphere Spectrometer and the epithermal and thermal neutron sensors, was observed, especially during the decrease and early recovery phase of the Forbush event, in contrast to quiet periods, where statistical fluctuations make the correlation less evident.

A clear increase of the Pearson r-coefficients during the Forbush period was quantified with respect to the pre-Forbush period, in all channels involving muons and neutrons with different energies, with a very slight predominance for neutrons of higher energy (NM and BSS sphere with the largest diameter), and the epithermal and thermal detector which can be ascribed to the lower signal to noise ratio given by a higher count rate.

The POLA-R detectors exhibited a faster recovery compared to neutron detectors with reliable count rates.

This analysis suggests a strategy for looking at correlations among various cosmic ray detectors, or among the rates of different secondary particles, exploiting Forbush periods as a boost to make even weak correlations more detectable with a higher sensitivity.

Possible future developments of this analysis will include the observation of this Forbush event with a set of MRPC telescopes of the EEE project, deployed over a large geographical area in Italy, thus allowing a combined analysis as a function of the observation latitude. Further correlation with the relevant solar parameters measured in the same period could also give further information on the evolution of catastrophic events in the Sun affecting the whole Earth.

Declaration of Competing Interest

The authors declare that they have no known competing financial interests or personal relationships that could have appeared to influence the work reported in this paper.

Acknowledgments

We thank the Istituto di Scienze Polari of the Consiglio Nazionale delle Ricerche (Institute of Polar Sciences, CNR-ISP) hosting the POLA-R detectors at the CNR facilities in Ny-Ålesund and the personnel of the Dirigibile Italia station as well as the AWIPEV stations for their help

in the management and monitoring of the detectors. Particular thanks goes to Werner Rühm (Bundesamt für Strahlenschutz) and Vladimir Mares (formerly Helmholtz Centre Munich) for setting up and operating the Bonner Sphere System since 2008.

We acknowledge the NMDB database www.nmdb.eu, funded under the European Union's FP7 programme (contract No. 213007) for providing data. Mexico City neutron monitor data were kindly provided by the Cosmic Ray Group, Geophysical Institute, National Autonomous University of Mexico (UNAM), Mexico.

We acknowledge the Polar Geophysical Institute for the data from the Barentsburg Neutron Monitor accessed through http://cr0.izmiran.ru/brbg/main.htm.

We also thank Paolo Romano for the access to the Solar Telescope archive of the Catania Astrophysical Observatory.

We thank AWIPEV (Alfred Wegener Institute for Polar and Marine Research and the French Polar Institute Paul-Émile Victor) for substantial support in the context of Grant No. AWIPEV_0017.

Funding was provided by the Research Council of Norway, project number 322387, Svalbard Integrated Arctic Earth Observing System - Knowledge Centre, operational phase 2022.

References

Abbrescia, M., Aiola, S., Antolini, R., Avanzini, C., Baldini Ferroli, R., Bencivenni, G., Bossini, E., Bressan, E., Chiavassa, A., Cicalo, C., et al., 2011. Observation of the February 2011 Forbush decrease by the EEE telescopes. Eur. Phys. J. Plus 126, 1–7.

Abbrescia, M., Avanzini, C., Arlandoo, M., Balbi, G., Baldini, L., Ferroli, R.B., Batignani, G., Battaglieri, M., Boi, S., Cavazza, D., et al., 2020. New high precision measurements of the cosmic charged particle rate beyond the Arctic Circle with the PolarquEEEst experiment. Eur. Phys. J. C 80, 1–20.

Abbrescia, M., Avanzini, C., Baldini, L., Baldini Ferroli, R., Batignani, G., Bencivenni, G., Bossini, E., Bressan, E., Chiavassa, A., Cicalo, C., et al., 2015. Results from the observations of Forbush decreases by the Extreme Energy Events experiment. Proc. Sci. SISSA, 1–8.

Abbrescia, M., Avanzini, C., Baldini, L., et al., 2018. The Extreme Energy Events experiment: an overview of the telescopes performance. J. Instrum. 13, P08026.

Ashrufayisha, M., 2024. Loss of 12 starlink satellites due to preconditioning of intense space weather activity surrounding the extreme geomagnetic storm of 10 May 2024. arXiv:2410.16254v1 [physics.space-ph] 21 Oct 2024.

Barbashina, N., Astapov, I., Borog, V., Dmitrieva, A., Kokoulin, R., Kompaniets, K., Kuzov, A., Petrukhin, A., Shutenko, V., Yakovleva, E., et al., 2011. Analysis of Forbush decrease of 18 february 2011 in muon flux. International Cosmic Ray Conference, p. 278.

Belov, A., 2008. Forbush effects and their connection with solar, interplanetary and geomagnetic phenomena. Proc. Int. Astron. Union, 4, pp. 439–450.

Bittner, M., 2022. Science at the environmental research station schneefernerhaus/zugspitze.

Boike, J., Juszak, I., Lange, S., Chadburn, S., Burke, E., Overduin, P.P., Roth, K., Ippisch, O., Bornemann, N., Stern, L., et al., 2018. A 20-year record (1998–2017) of permafrost, active layer and meteorological conditions at a high Arctic permafrost research site (Bayelva, Spitsbergen). Earth Syst. Sci. Data 10, 355–390.

Cane, H., Richardson, I., Von Rosenvinge, T., 1993. Cosmic ray decreases and particle acceleration in 1978–1982 and the associated solar wind structures. J. Geophys. Res.: Space Phys. 98, 13295–13302.

Cane, H., Richardson, I., Von Rosenvinge, T., 1996. Cosmic ray decreases: 1964–1994. J. Geophys. Res.: Space Phys. 101, 21561–21572.

Cid, C., Saiz, E., Guerrero, A., Palacios, J., Cerrato, Y., 2015. A carrington-like geomagnetic storm observed in the 21st century. J. Space Weather Space Climate 5, A16.

Clem, J.M., Dorman, L.I., 2000. Neutron monitor response functions, in: Cosmic Rays and Earth: Proceedings of an ISSI Workshop, 21–26 March 1999, Bern, Switzerland, Springer. pp. 335–359.

Cooke, D., Humble, J., Shea, M., Smart, D., Lund, N., Rasmussen, I., Byrnak, B., Goret, P., Petrou, N., 1991. On cosmic-ray cut-off terminology. Il Nuovo Cimento C 14, 213–234.

Forbush, S.E., 1937. On the effects in cosmic-ray intensity observed during the recent magnetic storm. Phys. Rev. 51, 1108.

Forbush, S.E., 1938. On world-wide changes in cosmic-ray intensity. Phys. Rev. 54, 975.

Freiherr von Forstner, J.L., Guo, J., Wimmer-Schweingruber, R.F., Hassler, D.M., Temmer, M., Dumbović, M., Jian, L.K., Appel, J.K., Čalogović, J., Ehresmann, B., et al., 2018. Using Forbush decreases to derive the transit time of ICMEs propagating from 1 AU to Mars. J. Geophys. Res.: Space Phys. 123, 39–56.

Grieder, P.K., 2023. Cosmic ray muons. Cosmic Ray Muogr., 33–84

Guo, J., Lillis, R., Wimmer-Schweingruber, R.F., Zeitlin, C., Simonson, P., Rahmati, A., Posner, A., Papaioannou, A., Lundt, N., Lee, C.O., et al., 2018. Measurements of Forbush decreases at Mars: both by MSL on ground and by MAVEN in orbit. Astron. Astrophys. 611, A79.

Hayakawa, H., Ebihara, Y., Mishev, A., Koldobskiy, S., Kusano, K., Bechet, S., Yashiro, S., Iwai, K., Shinbori, A., Mursula, K., et al., 2024. The Solar and Geomagnetic Storms in May 2024: A Flash Data Report. arXiv preprint arXiv:2407.07665.

Hubert, G., 2024. Analyses of continuous measurements of cosmic ray induced-neutrons spectra at the Concordia Antarctic Station from 2016 to 2024. Astropart. Phys. 159, 102949.

INAF, 2024. INAF Catania Astrophysical Observatory picture archive. https://solar.oact.inaf.it [Accessed: (Nov 08, 2024)].

IZMIRAN, 2024. Barentsburg Neutron Monitor webpage. URL: http://cr0.izmiran.ru/brbg/main.htm. [Accessed: (Nov 08, 2024)].

Köhli, M., Schrön, M., Zreda, M., Schmidt, U., Dietrich, P., Zacharias, S., 2015. Footprint characteristics revised for field-scale soil moisture monitoring with cosmic-ray neutrons. Water Resour. Res. 51, 5772–5790.

Kwak, J.S., Kim, J.H., Kim, S., et al., 2024. Observational Overview of the May 2024 G5-Level Geomagnetic Storm: From Solar Eruptions to Terrestrial Consequences. J. Astron. Space Sci. 41, 171.

Leuthold, G., Mares, V., Rühm, W., Weitzenegger, E., Paretzke, H., 2007. Long-term measurements of cosmic ray neutrons by means of a Bonner Spectrometer at mountain altitudes–first results. Radiat. Protect. Dosimetry 126, 506–511.

Light, C., Bindi, V., Consolandi, C., Corti, C., Freeman, C., Kuhlman, A., Palermo, M., Wang, S., 2020. Interplanetary coronal mass ejection associated Forbush decreases in neutron monitors. Astrophys. J. 896, 133.

Lockwood, J.A., 1971. Forbush decreases in the cosmic radiation. Space Sci. Rev. 12, 658–715.

Lockwood, M., Cowley, S., Sandholt, P., Lepping, R., 1990. The ionospheric signatures of flux transfer events and solar wind dynamic pressure changes. J. Geophys. Res.: Space Phys. 95, 17113–17135.

Mares, V., Schraube, H., 1994. Evaluation of the response matrix of a Bonner Sphere Spectrometer with LiI detector from thermal energy to 100 MeV. Nucl. Instrum. Methods Phys. Res., Sect. A 337, 461–473.

Mashao, D.C., Alton, T.L., Baird, F., Binnersley, C.L., Bradnam, S., Croft, S., Joyce, M., Packer, L., Ryden, K.A., Turner, T., et al., 2024. Observation of Forbush decreases and GLE-74 recorded during ground-level neutron monitoring survey from various sites across the British isles. Authorea Preprints.

Maturilli, M., 2024. Continuous meteorological observations at station Ny-Ålesund (2024–05). PANGAEA. https://doi.org/10.1594/PANGAEA.969445.

McDonald, F., Trainor, J., Webber, W., 1982. Pioneer and Voyager observations of Forbush decreases between 6 and 24 AU. In: in: 17th International Cosmic Ray Conference, pp. 147–150.

NMDB, 2024. Neutron Monitor Data Base. http://nmdb.eu [Accessed: (Nov 08, 2024)].

Norwegian Polar Institute, 2024. TopoSvalbard. URL: https://toposvalbard.npolar.no. accessed: (Nov 08, 2024).

Nwuzor, O., Okike, O., Umahi, A., Nwaevo, C., Nworie, C., Ojobeagu, A., Chikwendu, A., Ozibo, C., Otah, P., 2024. Investigating the Dependence of Forbush Decrease on Geomagnetic Cutoff Rigidity. Global J. Pure Appl. Sci. 30, 101–113.

Okike, O., Nwuzor, O., 2020. Investigation of the rigidity and sensitivity dependence of neutron monitors for cosmic ray modulation using algorithm-selected Forbush decreases. Mon. Not. R. Astron. Soc. 493, 1948–1959.

Pioch, C., Mares, V., Rühm, W., Iwase, H., Iwamoto, Y., Sato, T., Hagiwara, M., Satoh, D., Nakane, Y., Nakashima, H., et al., 2011. Calibration of a Bonner Sphere Spectrometer in quasi-monoenergetic neutron fields of 244 and 387 MeV. J. Instrum. 6, P10015.

Pioch, C., Mares, V., Vashenyuk, E., Balabin, Y.V., Rühm, W., 2011. Measurement of cosmic ray neutrons with Bonner Sphere Spectrometer and neutron monitor at 79 N. Nucl. Instrum. Methods Phys. Res., Sect. A 626, 51–57.

Poluianov, S., Batalla, O., 2022. Cosmic-ray atmospheric cutoff energies of polar neutron monitors. Adv. Space Res. 70, 2610–2617.

Pudovkin, M., Veretenenko, S., 1995. Cloudiness decreases associated with Forbush-decreases of galactic cosmic rays. J. Atmos. Terr. Phys. 57, 1349–1355.

Romano, P., Guglielmino, S.L., Costa, P., Falco, M., Buttaccio, S., Costa, A., Martinetti, E., Occhipinti, G., Spadaro, D., Ventura, R., et al., 2022. On the evolution of a sub-C class flare: a showcase for the capabilities of the revamped Catania Solar Telescope. Sol. Phys. 297, 1–14.

Rühm, W., Mares, V., Pioch, C., Weitzenegger, E., Vockenroth, R., Paretzke, H., 2009. Measurements of secondary neutrons from cosmic radiation with a Bonner Sphere Spectrometer at 79 N. Radiat. Environ. Biophys. 48, 125–133.

Schattan, P., Köhli, M., Schrön, M., Baroni, G., Oswald, S.E., 2019. Sensing area-average snow water equivalent with cosmic-ray neutrons: the influence of fractional snow cover. Water Resour. Res. 55, 10796–10812. https://doi.org/10.1029/2019wr025647.

Schrön, M., Zacharias, S., Womack, G., Köhli, M., Desilets, D., Oswald, S.E., Bumberger, J., Mollenhauer, H., Kögler, S., Remmler, P., et al., 2018. Intercomparison of cosmic-ray neutron sensors and water balance monitoring in an urban environment. Geoscient. Instrument., Methods and Syst. 7, 83–99.

Tulasi Ram, S., Veenadhari, B., Dimri, A., Bulusu, J., Bagiya, M., Gurubaran, S., Parihar, N., Remya, B., Seemala, G., Singh, R., et al., 2024. Super-intense geomagnetic storm on 10–11 May 2024: Possible mechanisms and impacts. Space Weather 22, e2024SW004126.

Usoskin, I., Braun, I., Gladysheva, O., Hörandel, J., Jämsén, T., Kovaltsov, G., Starodubtsev, S., 2008. Forbush decreases of cosmic rays: Energy dependence of the recovery phase. J. Geophys. Res.: Space Phys., 113

Verpoest, S., Soldin, D., Desiati, P., 2024. Atmospheric muons and their variations with temperature. Astropart. Phys. 161, 102985.

Zreda, M., Shuttleworth, W.J., Zeng, X., Zweck, C., Desilets, D., Franz, T., Rosolem, R., 2012. COSMOS: the COsmic-ray Soil Moisture Observing System. Hydrol. Earth Syst. Sci. 16, 4079–4099. https://doi.org/10.5194/hess-16-4079-2012.